analytical chemistry

Article

Cite This: Anal. Chem. 2019, 91, 6225−6232

pubs.acs.org/ac

Spatial Microanalysis of Natural $^{13}C/^{12}C$ Abundance in Environmental Samples Using Laser Ablation-Isotope Ratio Mass Spectrometry

Andrei Rodionov,[*,†,¶,#] Eva Lehndorff,[‡,#] Ciprian C. Stremtan,[§] Willi A. Brand,[∥] Heinz-Peter Königshoven,[⊥] and Wulf Amelung[†]

[†]Institute of Crop Science and Resource Conservation (INRES), Soil Science and Soil Ecology, University of Bonn, Nussallee 13, Bonn 53115, Germany

[‡]Soil Ecology, University of Bayreuth, Dr.-Hans-Frisch-Str. 1-3, Bayreuth 95448, Germany

[§]Teledyne CETAC Technologies, 14306 Industrial Road, Omaha, Nebraska 68144, United States

[∥]Max-Planck-Institute for Biogeochemistry, Beutenberg Campus, P.O. Box 100164, Jena 07701, Germany

[⊥]Feinmechanische Werkstatt, Institute of Physical and Theoretical Chemistry, University of Bonn, Wegeler Str. 12, Bonn 53115, Germany

Supporting Information

ABSTRACT: The stable $^{13}C/^{12}C$ isotope composition usually varies among different organic materials due to isotope fractionation during biochemical synthesis and degradation processes. Here, we introduce a novel laser ablation-isotope ratio mass spectrometry (LA-IRMS) methodology that allows highly resolved spatial analysis of carbon isotope signatures in solid samples down to a spatial resolution of 10 μm. The presented instrumental setup includes in-house-designed exchangeable ablation cells (3.8 and 0.4 mL, respectively) and an improved sample gas transfer, which allow accurate $\delta^{13}C$ measurements of an acryl plate standard down to 0.6 and 0.4 ng of ablated carbon, respectively (standard deviation 0.25‰). Initial testing on plant and soil samples confirmed that microheterogeneity of their natural $^{13}C/^{12}C$ abundance can now be mapped at a spatial resolution down to 10 μm. The respective $\delta^{13}C$ values in soils with C3/C4 crop sequence history varied by up to 14‰ across a distance of less than 100 μm in soil aggregates, while being partly sorted along rhizosphere gradients of <300 μm from *Miscanthus* plant roots into the surrounding soil. These very first demonstrations point to the appearance of very small metabolic hotspots originating from different natural isotope discrimination processes, now traceable via LA-IRMS.

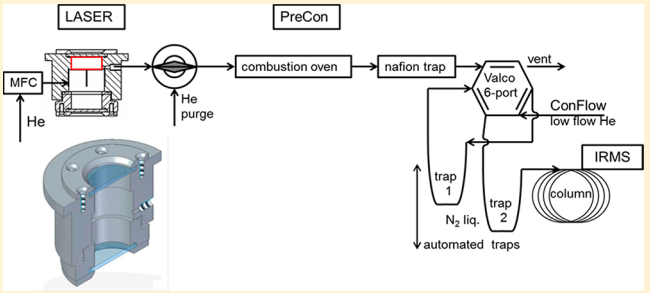

The stable $^{13}C/^{12}C$ isotope composition of environmental samples has become a unique tracer of carbon assimilation pathways. In plants, its analysis provided key information about the assimilation of fossil carbon sources (Suess effect)[1] and about differentiated C3 and C4 photosynthetic pathways[2,3] and gave hints regarding water stress adaptation pathways.[4−6] In marine and lacustrine environments, the analysis helped to track terrestrial C input and was useful for paleoclimate reconstruction.[7−9] In terrestrial environments, $\delta^{13}C$ analyses were indispensable for assessing the mean residence time of soil carbon after C3/C4 vegetation changes,[10,11] for elucidating microbial and faunal food webs,[12] and for paleo-environmental reconstructions.[13−16] However, spatially homogeneous C isotope signals were assumed for all these studies because it has not been possible to map microscale variation of the $^{13}C/^{12}C$ isotope composition in routine lab analyses down to the natural abundance level. The present contribution provides a viable solution to this problem.

Different instrumental setups using laser ablation (LA) combined with other detectors have already been applied on a micrometer scale for measuring bacterial cells and plant and animal tissue, as well as to other substances in geological and biological studies.[17−23] For ablation of organic matter, cold Nd:YAG laser ablation systems are recommended.[24,25] Lasers operating at 213 nm ensure cold ablation as more traditional 266 nm systems[24,25] and thus avoid isotope fractionation effects during the ablation process. All previous laser ablation studies relied on obtaining spatially resolved signatures from organic solids with relatively large and homogeneous organic C contents compared to soil (wood, single hair samples, or pollen grains of C3 and C4 plants), yielding ablation spot sizes between 150 and 50 μm[22,24,25] and a sensitivity between 65

Received: February 18, 2019
Accepted: April 1, 2019
Published: April 1, 2019

DOI: 10.1021/acs.analchem.9b00892
Anal. Chem. 2019, 91, 6225−6232

and 24 ng C.[25,26] Higher spatial resolution and sensitivity are crucial for many environmental studies, which have aims such as identifying microbial hotspots in soils and sediments, or patchy sequestration of carbon.

In this contribution, we introduce a laser ablation-isotope ratio mass spectrometry (LA-IRMS) system using a frequency quintupled 213 nm Q-switched Nd:YAG laser with <5 ns pulse width and flat-top energy profile (>4 mJ pulse^{-1}; Teledyne CETAC Technologies, Omaha, USA). Laser ablation of particulate matter was done in newly designed low-volume cells; the ablated particles were collected and transported using helium as the carrier gas. Particles were oxidized to CO_2 in an oven; then, sample gas was transferred to a system of two cryo-traps for gas cleanup and peak focus (modified PreCon system; see ref 27). Sample gas was then led through a GC column before it entered the IRMS DeltaVplus via a ConFloIV interface (both from ThermoFisher Scientific) for analysis of $\delta^{13}C$. The challenges were to increase the spatial resolution of the $\delta^{13}C$ signal by an order of magnitude by decreasing the area of ablated spots down to 10 μm, thus responding to a growing interest in isotopical characterization of microbial hot spots, organic exudates of roots, and residues of plants and microbes. Doing so would enable us to reach into areas where the utilization of organic materials is physically hindered by, e.g., encrustation processes and occlusion within aggregates and, thus, limited bioaccessibility.

EXPERIMENTAL APPROACH

Ablation System and Isotope Measurement. For laser ablation, highly focused laser light pulses are used to remove (ablate) material at a spatial resolution of a few micrometers in diameter from discrete areas of virtually any solid sample (e.g., ref 28 and references therein). For the present study, we used a Teledyne LSX-213G2+ solid state Nd:YAG laser system (CETAC, Omaha, NE, USA) that produces deep UV laser radiation at a wavelength of 213 nm. The laser pulse frequency can be variably adjusted; frequencies from 10 to 20 Hz proved to be optimal for this application. Furthermore, the laser allowed adjustment of the energy output, the ablated spot size, and the number of laser shots.

The standard cell of the LSX213 G2+ laser (two volume active cell HelEx II) was replaced with an in-house-designed single-volume cell (see Figure 1; the cell was constructed with an active volume of 3.8 cm^3 and a total internal volume of 17.2 cm^3; for details see Figure S-1). The cell was mounted on an adapted plane mount aligned to the laser's original movable stages, which allowed the sample to be monitored by a computer-controlled video microscope and internal LED illumination (coaxial, ring, and transmitted light sources). As we expected, the samples to have very low amounts of C, we also produced a second cell with the same design, but with an even smaller active volume of 0.4 cm^3 and, therefore, with reduced background signal. Both cells are easy to handle and are interchangeable.

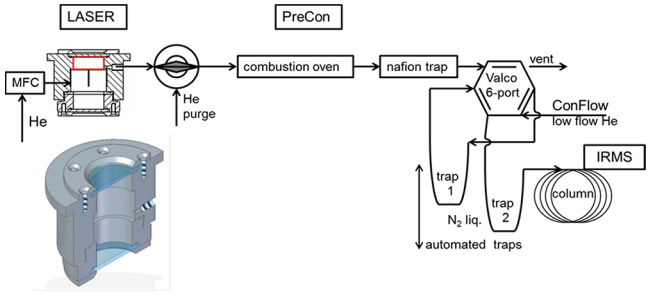

Figure 1. Setup of the LA-IRMS system starting with a newly constructed low-volume cell. Only the upper part of the cell is the active operating volume for laser ablation (marked in red; more details in the Supporting Information).

The upper and lower windows of the single-volume cell were made of quartz glass and sealed using O-rings (Ø30 × 2 mm; form error: 3/0.5 wedge: <5′; Laseroptik corp., Garbsen, Germany). The top window was specially coated (AR213 nm/0°; R < 0.25%) to reduce reflection of the 213 nm wavelength.

The system was continuously flushed with high purity helium (BIP5.0), which ran through a stainless steel line of 1/16 in., directly connected to a mass flow controller (MFC adjusted to constant flow rate of 10 mL min^{-1}; Alicat, Cole-Palmer, Vernon-Hills, IL, USA) and a PEEK 1/16 in. line between the MFC and the cell (Figure 1).

The resin-embedded sample was positioned on a spring inside the cell to reduce the cell's active volume (see Figure S-1; sample was embedded in Araldite 2020, Huntsman, $\delta^{13}C$ −29.98 ± 0.5‰, and then cut and polished with corundum to avoid C contamination on the sample surface). Helium was purged with 10 mL/min into the passive volume of the cell and then directed via four channels to the active cell volume above the sample. These four channel outlets were tilted (with 45° to the cell radius) to ensure gas rotation on the sample surface, thus increasing flow dynamics and particle suspension in the gas phase. The maximum sample diameters were 25 and 10 mm (3.8 and 0.4 cm^3 cell volume), respectively, which corresponds to sample sizes used in other applications, such as nanoscale secondary ion mass spectrometry (NanoSIMS).

The output port was laterally aligned close to the sample surface to increase particle collection efficiency (Figure S-1). This port was coupled to an IRMS via a PreCon automated interface, equipped with a continuous gas flow combustion furnace. The furnace was used to convert the carbon in the ablated sample to CO_2 at 900 °C. Low cell volumes allowed the oxidation of the complete sample in the oven. A Nafion trap was installed after the furnace to eliminate remaining traces of water. This was followed by cryo-trapping of the evolved CO_2 in a first automated trap using liquid nitrogen (Figure 1). The second automated trap focused the CO_2. After switching the Valco valve, both traps were purged with a reduced He flow, now received from the ConFlo interface (He flow of approximately 0.3 mL min^{-1}). Sample gas was then led through a capillary column for further cleanup and peak shaping (PoraPLOT Q, 25 m length, 0.25 mm diameter, 8 μm film; Agilent Technologies, Santa Clara, CA, USA) to a ConFlow and Delta V plus IRMS detector (Figure 1; ThermoFisher Scientific, Bremen, Germany). During sample exchange and stand-by, an additional He flow was added through the PreCon system (He purge at 10 psi, Figure 1) to ensure continuous He flow through the combustion furnace and lines (for stand-by, helium flow from the laser MFC had to be reduced to 3 mL min^{-1} to avoid overpressure at the laser (max. 19 psi)). To maintain the oxidizing capacity of the combustion, the furnace was periodically oxidized by using a Crystal-mix (Helium N46 mixed with 5.0 ± 0.1 Vol% Oxygen N45).

For accurate isotope ratio assessment, we used the Isodat Software (ThermoFisher Scientific), which basically starts each run with a peak center adjustment. Then, three peaks of CO_2

DOI: 10.1021/acs.analchem.9b00892
Anal. Chem. 2019, 91, 6225−6232

reference gas were introduced before sample ablation started. Directly before sample gas analysis, the IRMS performance was again checked by two CO_2 reference peaks (reference gas switched in through ConFloIV after cryo-trapping). The complete analytical procedure was programmed via an ISL protocol embedded in the Isodat software, which enables timing of valve position change, ConFloIV action (CO_2 reference gas inlet/sample gas inlet), and positioning of cryo-traps. The laser was controlled via the Chromium2.2 software (Laser Ablation System V.2017.1.31.0), and the ablation was started manually to work in time with the IRMS part of the LA-IRMS system. Each sample run needed about 10 min.

Standards and Reference Samples. For calibration of the CO_2 gas tank and reference samples, we used isotope reference standards reported versus Vienna PeeDee Belemnite (vs VPDB; acetanilide −29.53‰; cellulose −24.72‰; sucrose −10.45‰; National Institute of Standards and Technology, Gaithersburg, MD, USA), measured on a FlashEA 1112 elemental analyzer connected to a Delta V advantage IRMS (ThermoFisher Scientific, Bremen, Germany). In-house EA-IRMS referenced samples, which were chosen to resemble different types of organic matter occurring in soil, were applied to test the LA-IRMS system (beech wood −27.09 ± 0.02‰; einkorn wheat −28.71 ± 0.03‰; acryl plate −29.75 ± 0.06‰; IAEA-CH-3−24.77 ± 0.06‰; sucrose −26.93 ± 0.05‰; *Gordonia alcanivorans* −23.07 ± 0.00‰).

For the ablation tests, we produced press-pellets from each separate and in-house-referenced sample. With the exception of the IAEA-CH-3 standard[29] (which was cut into pieces), all samples were thoroughly homogenized to avoid any inconsistencies. The standards were placed in stainless steel sample holders in order to avoid any cross contamination (Figure S2). Each sample was ablated several times to test the effects of laser energy efficiency, as well as to try and correlate ablation depth to the number of shots.

Environmental Samples. To illustrate the performance of our LA-IRMS system, we used the following sample sets: (1) We assessed the carbon isotope composition in so-called occluded large microaggregates (53−250 μm), isolated from wet fractionated and ultrasonically treated macroaggregates (250−8000 μm). Such aggregates are considered to play a key role in C sequestration processes in soil because they protect physically occluded C from decay. (2) We assessed the carbon isotope signature along gradients from C4 roots (*Miscanthus*) into the surrounding soil (previously under C3 vegetation), with the knowledge that the living area around roots (the so-called rhizosphere) is a hot spot for microbial activity, thus inducing steep gradients in carbon concentration and its turnover. (3) We assessed the spatial variability of carbon isotope composition in soil particles <2 mm, which have received C inputs by C3 and C4 vegetation (two years after C3 to C4 vegetation change).

Soil microaggregates (set 1) were formed in arable loamy Haplic Luvisols (35% clay; 5−15 cm sampling depth, Scheyern experiment station, Southern Germany).[30]

Topsoil samples from a *Miscanthus* field (set 2) were collected from the experimental research station of Bonn University in Klein-Altendorf, Germany, continuously cropped with *Miscanthus* since 2007. Coordinates were 50°35′37.18 N/6°59′10.24 E at an altitude of 240 m a.s.l. The mean annual temperature and precipitation were 9.5 °C and 605 mm. The main soil type was a Luvic Stagnosol (Episiltic) (IUSS Working Group WRB, 2015), with a silty-loam texture (63% silt, 23% clay, and 14% sand).[31]

For set 3, soil particles <2 mm from a C3/C4 vegetation change experiment at the Terrestrial Observatory TERENO, Selhausen, Germany, were sampled in 2014 (0−30 cm soil depth). Soil had been continuously cropped with maize since 2012 (*Zea mays* L.).[32] The mean annual temperature and precipitation were 9.8 °C and 693 mm, respectively. The main soil type was a Stagnic Cambisol (Skeletic) (IUSS Working Group WRB, 2015) with a silty-loam texture (64% silt, 15% clay, and 18% sand).[32]

Environmental samples were taken as large blocks with a spade. They were manually broken to undisturbed aggregates of approximately 15 mm in diameter and air-dried (set 2), further processed using wet sieving into different aggregate size classes and freeze-dried (set 1),[30] or simply dry-sieved to 2 mm (set 3).[32] The dried subsamples were then embedded in Araldite before analysis.

Surface Mapping. To determine the ablation quality and to assess the crater depth and amount of ablated material, noncontact 2D and 3D surface mappings were applied to the acryl plate in-house standard. The measurements were carried out using an Omniscan MicroXAM white lite roughness microstitching interferometer (ADE Phase Shift, Tucson, AZ, USA) at Trinity College Dublin Center for Microscopy and Analysis. The repeated measurements of the crater depths were performed on combinations of ablation spot size with number of shots (Figure S3; Table S1; n = 5).

RESULTS AND DISCUSSION

Blank Minimizing through Sample Aerosol Transport Optimization. There is a general risk that CO_2 from sources other than the sample may contribute to the assessment of $\delta^{13}C$ values by LA-IRMS. We call this the blank signal, originating from small amounts of CO_2 already present in the cell, entering through the Valco-6-port connector, or resulting from other tiny leakages in the system. Thus, the isotope discrimination tests were performed at C concentrations far above the blank signal. However, to perform accurate LA-IRMS analyses at very low C concentrations at high spatial resolution, minimization of the blank signal was crucial. We observed that its contribution to the total signal increased with increasing loading time on the cryo-trap (Figure 2). However, the isotope composition of the blank was not affected by the loading time. It averaged −18.78 ± 0.54‰, ranging from

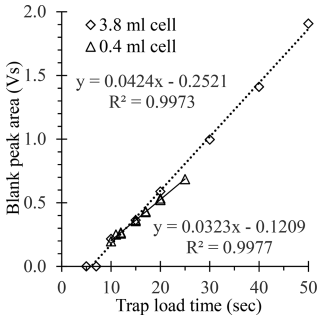

Figure 2. Impact of loading time in the first cryo-trap on the blank peak area in cells with 3.8 and 0.4 mL active volume (without laser ablation). If the loading time was <7 s, the blank was at the baseline level of the IRMS detector for both cells. The isotopic signature of the blank signal was not affected by the loading time.

DOI: 10.1021/acs.analchem.9b00892
Anal. Chem. 2019, 91, 6225−6232

−17.93‰ to −19.27‰ on different days (n = 34; individual data not shown). With the 3.8 mL cell and a trap loading time of 7 s, the blank fell below the routine detection limit of the IRMS system (which was preset to 50 mV; that is, close to the baseline). With a loading time of 20 s, the blank signal remained stable with a peak area less than 0.6 Vs; this means that any signal above this value must have resulted from sample ablation. Thus, very clear ablation signals from the in-house acryl standard were produced with spots of 30 μm size and 40 shots in a 3.8 mL cell volume (Figure S-4). By minimizing the time window for cryo-trapping, that is, finding the optimum delay time between particle ablation in the cell and particle arrival at trap 1 (loading time), the blank signal could be reduced significantly as needed for improved sensitivity. All these steps were controlled by the Valco-6-port valve in the PreCon settings (modified ISL method of the PreCon, loaded in the Isodat Software, ThermoFisher Scientific). The method was programmed with a delay time of 2 s until switching to cryo-trapping with a loading time of 20 s for the 3.8 mL cell (see details for the 0.4 mL cell below).

Energy Efficiency and Limitation of the Fractionation. First, we tested the optimal efficiency of the LA-IRMS system under different ablation settings and for different in-house standardized organic materials with known δ^{13}C value, such as beech wood, sucrose, einkorn grass, the actinomycete *Gordonia alcanivorans*, an acryl plate, and the certified IAEA-CH-3 standard. The question was whether these organic materials, which commonly occur in soil, show different ablation behavior. To perform these tests, we produced press-pellets from milled standard materials and placed them in the metal sample holders (Figure S-1a,b). According to Jeong et al.,[33] the entrainment efficiency of particle transport decreases with increasing laser power density and is strongly affected by laser beam diameter at constant laser pulse energy (that is, removing more sample than can be efficiently collected and transported) or at variable laser pulse energy with fixed spot size. We tested the appropriate laser pulse energy using a fixed spot size and a fixed number of shots in increments, starting from the configuration of 40% energy output to 20%, 15%, 10%, 5%, and finally 3.5% energy output (Figure 3). Using a constant spot size of 30 μm and 40 pulses, the results of different in-house-referenced samples clearly showed that the 3.5% energy output setting of the laser (corresponding to a fluence of 0.71 J/cm^2) was appropriate for organic matter ablation independent of matrix. If higher laser energies were set, δ^{13}C decreased from the referenced value, probably due to partial heating of the sample inducing isotopic discrimination (Figure 3). Also, the blank contribution was significantly reduced and, since this was constant during the day, it did not interfere with the sample measurements. Across different days, however, the isotope composition of the blank varied, which must be accounted for when analyzing a sample at different days (Figure 3).

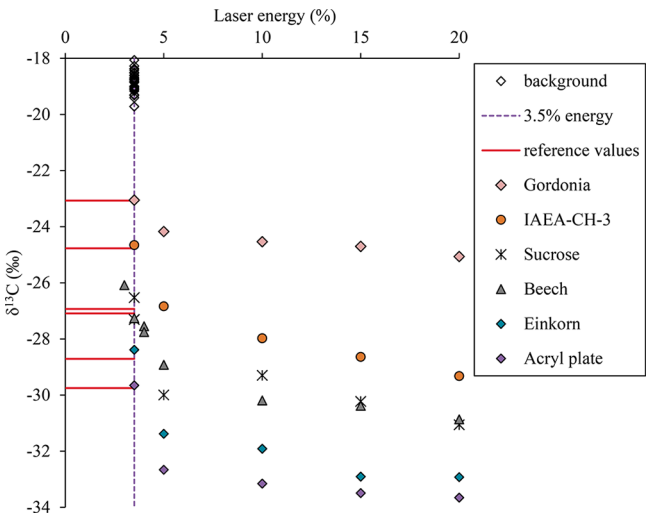

Figure 3. Discrimination of stable carbon isotopes from different organic matrices by ablation with increasing laser energy.

Sensitivity. The sensitivity of the LA-IRMS system was tested by applying variable spot sizes (40, 30, 25, 20, 15, and 10 μm) and numbers of pulses (40, 30, 20, and 10 shots) to our organic matrices (cell size 3.8 mL, Figure S-4a,b). As expected, the results showed that decreasing the spot size impacted the resulting signal intensity more than a decreasing number of shots. The combination of both, that is, the dilution of the blank signal in a sample by increasing the sample volume, resulted in a linear decrease of the measured isotope signal for all tested in-house-referenced samples ($\Delta\delta^{13}C = \delta^{13}C_{total} - \delta^{13}C_{reference}$; Figure S-4a; Table S1). In the 3.8 mL cell, the isotope signal was stable for 30 μm spots due to a negligible blank signal, and the resulting isotope signatures were close to the reference values (Figure S-4b).

Here, we directly measured the blank value and subtracted the respective contribution of blank carbon from sample carbon. In detail, this means that, when ablating soil samples, we need to compare the resulting carbon signature with that of the reference peak from standard material that was homogeneous in carbon content. The subtraction then refines the resulting signals by a linearity correction, which involves using measured and true values for the CO_2 reference gas.

A blank correction for isotope ratio measurement with small amounts of samples can be performed by regression or by subtraction[34,35] and calculated as described by Werner et al.:[36]

$$\delta^{13}C_{sample} = \frac{(\delta^{13}C_{total} \times A_{total} - \delta^{13}C_{blank} \times A_{blank})}{(A_{total} - A_{blank})}$$

where A is the area of the m/z 44 peak.

The trapping time of 20 s needed for the complete transport of the sample gas suspension from a 3.8 mL cell to the first cryo-trap poses a constraint for sampling resolution; namely, the signal intensity from ablated carbon material had to be in excess of 0.3 Vs for it to be reproducible (Figure S-4b).

To calculate the ablated C amount, we used an acryl plate and measured the total ablated volume (Figure S-3a; C content 60%; density 1.19 g cm^3; $\delta^{13}C_{Acryl}$ = −29.75 ± 0.06‰, relative to VPDB using EA-IRMS). We determined the ablated crater volume for different combinations of laser spot size and shot numbers (Figure S-3b; Table S1). The crater geometry and overall symmetry may influence the depth resolution and fractionation effects, which might not be strictly related only to the beam profile. The Nd:YAG laser was able to produce flat-bottom and straight-wall craters.[37,38] The crater geometry (Figure S-3b,c) maintained flat-bottom laser beam profiles during repeated ablations at a single spot, using focused laser light pulses with 10 and 40 μm operative diameters. Because of this crater assessment, we were able to calibrate the LA-IRMS signal to C amount and, thus, also determine sample size requirements for the reference measurements comparable to

DOI: 10.1021/acs.analchem.9b00892
Anal. Chem. 2019, 91, 6225−6232

Moran et al.[25] The final limit of determination corresponded to a carbon amount of 0.6 ng for the 3.8 mL cell, which corresponded to a minimum of 20 μm ablated spot size (Figure 4a).

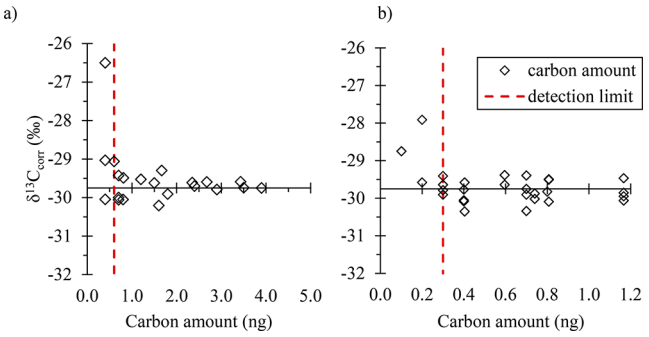

Figure 4. Detection limit of the LA-IRMS system given in C amount (a) for the cell with 3.8 mL active volume and (b) for the cell with 0.4 mL active volume (detected with an acryl plate with known ablated crater volume; see also Supporting Information).

Sensitivity Enhancement. In order to be able to detect carbon when using spots <20 μm in diameter, we built a second sample cell with reduced active volume (0.4 mL). We used it with decreased loading time for cryo-trapping in order to minimize blank signal accumulation in the cryo-traps (Figure 2). The isotopic signature of the blank was comparable to that of the 3.8 mL cell, but the contribution of the blank to the ablated signal was significantly smaller. The trapping time needed for the evacuation (transport efficiency) of the sample was best at 10 s (Figure S-5). A saturation of raw isotopic signal from the acryl plate was reached at a δ-value of −37.42 ± 0.37‰, irrespective of the loading time; this indicates that the blank contribution could then be neglected (Figure S-5a). The smaller cell finally yielded the same δ^{13}C values as the larger cell after blank correction (Table 1; Table S-1). We conclude that operation with the small cell is feasible, which enables us to reduce the combination of spot size for laser ablation to 15 μm with 20 shots and to 10 μm with 40 shots. The limit of determination was calculated to be 0.3 ng C for the 0.4 mL cell, which corresponded to a minimum ablated spot size of 10 μm (Figure 5b).

Analyses of Environmental Samples. We first applied our methodology to soil microaggregates (sample set 1, long-term arable experiment station at Scheyern, Germany). We fixed the occluded microaggregate fraction in Araldite and detected spotwise the δ^{13}C using the 3.8 mL cell (Figure 5). During the analyses of the embedded material, we randomly repeated the acryl plate standard measurement in order to have the reference measurements in the same sample run (Figure S-2c). The bulk soil and microaggregate fraction (53−250 μm) were characterized for their C isotope composition before using EA-IRMS and showed an average δ^{13}C value of −25.10 ± 0.07‰ and −25.36 ± 0.42‰, respectively. However, the single isotopic signals in the ablated material showed a much larger variability, which reached a data spread >1‰ independent of ablation spot size (Table 2). In soil, such a shift in δ^{13}C values corresponds to organic matter degradation along a depth interval of a few dm in native sites not experiencing a C3/C4 vegetation change, which may well comprise >1000 years of organic matter turnover and genesis.[39] Therefore, the accuracy of δ^{13}C analyses for bulk soil or even a soil aggregate fraction in no way represents the true heterogeneity of processes involved in soil organic matter transformation and genesis. Instead, we have to conclude that there are hot spots of C accrual, even at microaggregate level, that originate from different isotope discrimination processes and, thus, probably from different organic molecules and, respectively, from different plant or microbial debris.

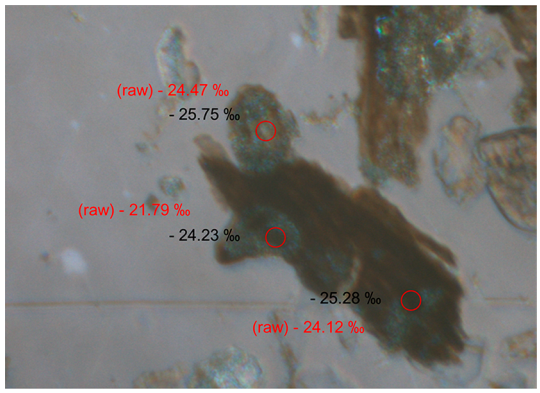

Figure 5. Spatially resolved microanalysis of δ^{13}C heterogeneity in a soil microaggregate structure from a cropped Luvisol field of 33% clay (53−250 μm aggregate fraction, 20 μm spot size, 40 shots per ablation). Raw δ^{13}C values shown in red and blank corrected δ^{13}C values, in black.

Heterogeneous δ^{13}C distribution not only is to be expected in soils but also has previously been found for tree rings[24] and may be expected as well for root exudation of C into soil as for nutrient uptake and related feeding of the microbial community. We detected the microscale shift in C isotope composition in a gradient ablated from the root to the root-to-soil contact zone (rhizosphere) and the soil matrix (Figures 6a,b and S-6). The root, which was from *Miscanthus* (sample set 2), clearly consisted of C4-photosynthesis derived C (with an average δ^{13}C of −19‰, Figure 6a), while soil in about 300 μm distance did not yet show signs of C4-carbon input. However, signals had already mixed in less than a 300 μm

Table 1. Accuracy Tests of the LA-IRMS System with 3.8 and 0.4 mL Active Cell Volume

	laser ablation-IRMS							
	active volume 3.8 mL			active volume 0.4 mL			EA-IRMS	
sample	δ^{13}C ± st.dev. (‰)	offset (‰)	n	δ^{13}C ± st.dev. (‰)	offset (‰)	n	δ^{13}C ± st.dev. (‰)	n
acryl plate[a]	−29.68 ± 0.25	−0.07	39	−29.77 ± 0.25	0.02	22	−29.75 ± 0.06	5
IAEA-CH-3	−24.72 ± 0.78	0.00[b]	30	−24.80 ± 0.57	0.08[b]	21	−24.77 ± 0.06	5
Beech	−27.05 ± 0.64	−0.04	27				−27.09 ± 0.02	5

[a]Acryl plate sampling corresponded to 3.4 ng C in the 3.8 mL cell and 0.7 ng C in the 0.4 mL cell (see text for calculation). [b]IUPAC reference for δ^{13}C value IAEA-CH-3 = −24.72 ± 0.04‰.[29]

DOI: 10.1021/acs.analchem.9b00892
Anal. Chem. 2019, 91, 6225−6232

Table 2. $\delta^{13}C$ in Spots Ablated with 20 and 30 μm Spot Size from Soil Microaggregates[a]

fraction [μm]	spot size [μm]	LA-IRMS $\delta^{13}C$ [‰]	EA-IRMS $\delta^{13}C \pm$ s.d. [‰]
<2000			−25.10 ± 0.07
250−53 occluded	20	−25.28	−25.36 ± 0.42
		−23.59	
		−26.83	
		−25.28	
		−24.23	
		−25.36	
		−25.21	
250−53 occluded	30	−27.36	
		−26.68	
		−23.90	
		−25.60	
		−24.98	
		−25.13	

[a]Laser ablation revealed high spatial variability, which is not visible from standard EA-IRMS analysis. The $\delta^{13}C$ was not influenced by spot size (3.8 mL cell active volume, mean isotope signal from 13 LA-IRMS measurements −25.34 ± 1.11‰ compared well to bulk sample EA-IRMS analysis).

distance, indicating that 25−50% of the C was gradually exchanged in this region. To our knowledge, this is the very first in situ detection of rhizosphere gradients using stable-isotope screening. Rhizosphere gradients evolve because of water and related nutrient uptake, which eventually cost carbon to feed the nutrient-mobilizing community and are frequently assumed to extend into a gradient of up to 1−4 mm. Figure 6a suggests that rhizosphere extension in terms of C exudation from roots to soil may even be limited to 100 μm, that is, very close to the rhizoplane. These findings shed new light on rhizosphere biochemistry, since getting hold of its extension has challenged research until now (e.g., ref 40).

When using the same embedded material, but decreasing spot size to 10 μm, even a larger range of $\delta^{13}C$ isotope values was found (Figure 6b). This range reached 13.76‰, which was slightly larger than the range detected with a spot size of 15 μm ($\Delta\delta^{13}C$ = 13.25‰). While this may still be due to random hits of different hot spots in soil, none of the δ-values above −17‰ (Figure 6b) had been found using 30 μm-sized spots (Figure 6a). We attribute this to the improvement of our cell: only a spot size of 10 μm is able to discover the full range of isotope values in the environment (here, soils with C3/C4 vegetation change), while a spot size of 30 μm already includes the risk of averaging across a sampling area that is too large to detect realistic hot spots. As former attempts to track $\delta^{13}C$ values in plant and soil had to rely on a spot size of at least 100−150 μm (e.g., ref 23), we see our method developments as a clear step toward a now upcoming, in situ mapping of $\delta^{13}C$ isotope values and discrimination processes in the environment.

In order to obtain an independent field replicate, we took another sample from 2 years of the C3/C4 vegetation change from the Terrestrial Observatory TERENO Selhausen, Germany.[3,32] Even though we only performed laser shots on sieved soil aggregates, we detected the full range of possible $\delta^{13}C$ values, reflecting hotspots of both C3 and C4 plant origin (Figure 7). Again, this discovered range was almost as large as

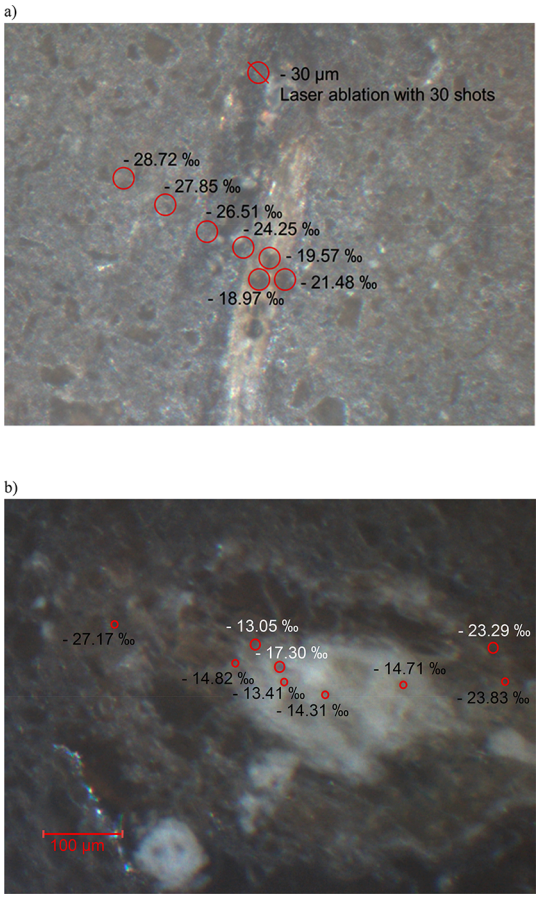

Figure 6. Spatial differences of isotopic signatures inside the root, rhizosphere area, and soil matrix from a *Miscanthus* root ablated with (a) constant spot size of 30 μm and 30 shot numbers and with (b) variable spot size of 15 μm and 40 shot numbers (white-colored signatures) and spot size of 10 μm and 80 shot numbers (black colored signatures), both performed on a 60 μm cross section; in-house reference acryl = −29.75 ± 0.04‰.

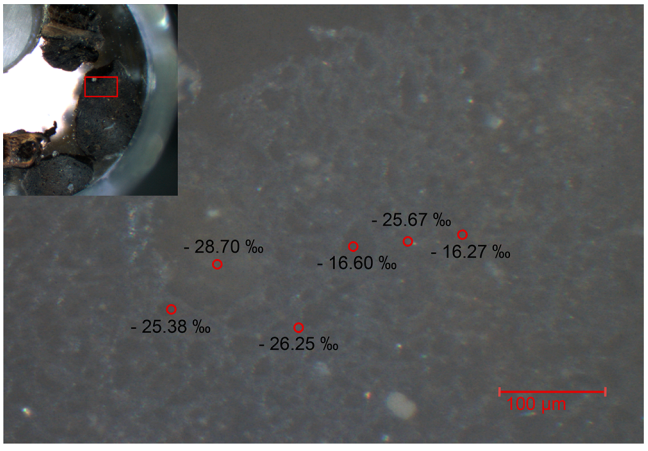

Figure 7. Spatial differences of isotopic signatures ablated from 2 mm sieved soil with constant spot size of 10 μm and 60 shot numbers after 2 years of C3 to C4 vegetation change (*Zea mais* L., Selhausen; in-house reference acryl = −29.57 ± 0.32‰).

the difference between C3 and C4 plant species ($\Delta\delta^{13}C$ = 12.44‰), even though the hot spots looked macroscopically similar. The results have two implications. From an analytical point of view, these data show that it is possible to resolve hot

DOI: 10.1021/acs.analchem.9b00892
Anal. Chem. 2019, 91, 6225−6232

spots of C accrual with different ^{13}C isotope discrimination in an environment even down to a spatial scale of 10 μm. From the environmental point of view, the data implies that it is possible to find microsites at which original C3 plant material had remained untouched in soil, while other places were comprised solely of the newly C4 carbon introduced; in other words, there are microsites with more or less 0−100% of C sequestration, separated by a distance of only a few micrometers.

CONCLUSIONS AND IMPLICATIONS

By adapting laser ablation isotope ratio monitoring to $\delta^{13}C$ analysis in soil organic matter on the microscale, we found significant heterogeneity in soil microaggregates after C3/C4 vegetation change (>10‰), as well as in microaggregates that did not receive a vegetation change (3‰), and we were able to detect C4−C inputs from roots into soil. Hence, this technique allows us to spatially recognize hot spots of organic C turnover in soil, as well as of input dimensions of rhizodeposits and root exudates. The same will be possible in other environmental samples like sediments, geological and geoarcheological archives, or biological tissues. The achieved current spot size of 10 μm allows detection of natural $\delta^{13}C$ abundance far below conventional IRMS routines, which is achieved here by minimizing the split of sample gas fluxes and by reducing active cell volume to 3.8 and 0.4 mL. Future challenges might be the automatization of the ablation procedure (communication between laser and IRMS equipment) and the extension to $\delta^{15}N$ analysis, which requires a modified analytical setup for focusing on the N_2 peak.

ASSOCIATED CONTENT

Supporting Information

The Supporting Information is available free of charge on the ACS Publications website at DOI: 10.1021/acs.analchem.9b00892.

One table and six figures showing the determination of carbon amount by measurements of crater depth on an acryl plate (Table S-1), configuration of the newly developed laser cells (Figure S-1), images of press-pellets from the ground and mixed standard substances (Figure S-2), images of spot depth and surface mapping of ablated spots (Figure S-3), deviation of the $\delta^{13}C$ signal from referenced values due to the contribution of the blank signal (Figure S-4), adjustment of loading times in the cryo-trap (Figure S-5), and stable C isotope signatures of a *Miscanthus* rhizome and the surrounding soil (Figure S-6) (PDF)

AUTHOR INFORMATION

Corresponding Author

*E-mail: andrey.rodionov@uni-bayreuth.de.

ORCID

Andrei Rodionov: 0000-0001-5971-1948

Present Address

¶A.R.: Soil Ecology, University of Bayreuth, Dr.-Hans-Frisch-Str. 1-3, 95448 Bayreuth, Germany.

Author Contributions

#A.R. and E.L. shared first authorship.

Notes

The authors declare no competing financial interest.

ACKNOWLEDGMENTS

We acknowledge the technician, Leona O'Connor, at Trinity College Dublin Center for Microscopy and Analysis, for performing the surface measurements. We also wish to thank members of the staff at Steinmann Institute, Nils Jung and Thomas Schulz at the University of Bonn, and Raphael Njul at the Bavarian Research Institute of Experimental Geochemistry and Geophysics (BGI), University of Bayreuth, for their support of the sample embedding and preparation. This work is associated with the MAD Soil project, which was funded by the DFG (Deutsche Forschungsgemeinschaft, Research Unit 2179). We very much acknowledge the help of two anonymous reviewers.

REFERENCES

(1) Köhler, P. *Environ. Res. Lett.* **2016**, *11*, 124016.
(2) Beer, K. D.; Orellana, M. V.; Baliga, N. S. *Cell* **2013**, *153*, 1427−1429.
(3) Kellogg, E. A. *Curr. Biol.* **2013**, *23*, R594−9.
(4) Moreno-Gutiérrez, C.; Dawson, T. E.; Nicolás, E.; Querejeta, J. I. *New Phytol.* **2012**, *196*, 489−496.
(5) Gebrekirstos, A.; van Noordwijk, M.; Neufeldt, H.; Mitlöhner, R. *Trees* **2011**, *25*, 95−102.
(6) Hartman, G.; Danin, A. *Oecologia* **2010**, *162*, 837−852.
(7) Hudson, A. M.; Quade, J.; Ali, G.; Boyle, D.; Bassett, S.; Huntington, K. W.; De los Santos, M. G.; Cohen, A. S.; Lin, K.; Wang, X. *Geochim. Cosmochim. Ac.* **2017**, *212*, 274−302.
(8) Wilson, K. E.; Maslin, M. A.; Leng, M. J.; Kingston, J. D.; Deino, A. L.; Edgar, R. K.; Mackay, A. W. *Geology* **2014**, *42*, 955−958.
(9) Laskov, C.; Amelung, W.; Peiffer, S. *Environ. Sci. Technol.* **2002**, *36*, 4218−4223.
(10) Derrien, D.; Amelung, W. *Europ. J. Soil Sci.* **2011**, *62*, 237−252.
(11) Still, C. J.; Berry, J. A.; Collatz, G. J.; DeFries, R. S. *Global Biogeochem. Cycles* **2003**, *17*, 6-1−6-14.
(12) Blagodatskaya, E.; Yuyukina, T.; Blagodatsky, S.; Kuzyakov, Y. *Soil Biol. Biochem.* **2011**, *43*, 159−166.
(13) Schemmel, F.; Mikes, T.; Rojay, B.; Mulch, A. *Am. J. Sci.* **2013**, *313*, 61−80.
(14) Leier, A.; Quade, J.; DeCelles, P.; Kapp, P. *Earth Planet. Sci. Lett.* **2009**, *279*, 242−254.
(15) Sikes, N. E.; Ashley, G. M. *J. Hum. Evol.* **2007**, *53*, 574−594.
(16) Sankaran, M.; Hanan, N. P.; Scholes, R. J.; Ratnam, J.; Augustine, D. J.; Cade, B. S.; Gignoux, J.; Higgins, S. I.; Le Roux, X.; Ludwig, F.; Ardo, J.; Banyikwa, F.; Bronn, A.; Bucini, G.; Caylor, K. K.; Coughenour, M. B.; Diouf, A.; Ekaya, W.; Feral, C. J.; February, E. C.; Frost, P. G. H.; Hiernaux, P.; Hrabar, H.; Metzger, K. L.; Prins, H. H. T.; Ringrose, S.; Sea, W.; Tews, J.; Worden, J.; Zambatis, N. *Nature* **2005**, *438*, 846−849.
(17) van Malderen, S. J. M.; Laforce, B.; van Acker, T.; Vincze, L.; Vanhaecke, F. *J. Anal. At. Spectrom.* **2017**, *32*, 289−298.
(18) van Malderen, S. J. M.; Vergucht, E.; De Rijcke, M.; Janssen, C.; Vincze, L.; Vanhaecke, F. *Anal. Chem.* **2016**, *88*, 5783−5789.
(19) Wu, B.; Becker, J. S. *Int. J. Mass Spectrom.* **2011**, *307*, 112−122.
(20) Limbeck, A.; Galler, P.; Bonta, M.; Bauer, G.; Nischkauer, W.; Vanhaecke, F. *Anal. Bioanal. Chem.* **2015**, *407*, 6593−6617.
(21) Scarciglia, F.; Barca, D.; De Rosa, R.; Pulice, I. *Geoderma* **2009**, *152*, 113−126.
(22) Spötl, C.; Mattey, D. *Chem. Geol.* **2006**, *235*, 48−58.
(23) Bruneau, P. M. C.; Ostle, N.; Davidson, D. A.; Grieve, I. C.; Fallick, A. E. *Rapid Commun. Mass Spectrom.* **2002**, *16*, 2190−2194.
(24) Schulze, B.; Wirth, C.; Linke, P.; Brand, W. A.; Kuhlmann, I.; Horna, V.; Schulze, E.-D. *Tree Physiol.* **2004**, *24*, 1193−1201.
(25) Moran, J. J.; Newburn, M. K.; Alexander, M. L.; Sams, R. L.; Kelly, J. F.; Kreuzer, H. W. *Rapid Commun. Mass Spectrom.* **2011**, *25*, 1282−1290.
(26) van Roij, L.; Sluijs, A.; Laks, J. J.; Reichart, G.-J. *Rapid Commun. Mass Spectrom.* **2017**, *31*, 47−58.

DOI: 10.1021/acs.analchem.9b00892
Anal. Chem. 2019, 91, 6225−6232

(27) Brand, W. A. *Isot. Environ. Health Stud.* **1995**, *31*, 277−284.
(28) Günther, D.; Hattendorf, B. *TrAC, Trends Anal. Chem.* **2005**, *24*, 255−265.
(29) Brand, W. A.; Coplen, T. B.; Vogl, J.; Rosner, M.; Prohaska, T. *Pure Appl. Chem.* **2014**, *86*, 425−467.
(30) Krause, L.; Rodionov, A.; Schweizer, S. A.; Siebers, N.; Lehndorff, E.; Klumpp, E.; Amelung, W. *Soil Tillage Res.* **2018**, *182*, 123−129.
(31) Glisczynski, F. v.; Pude, R.; Amelung, W.; Sandhage-Hofmann, A. *J. Plant Nutr. Soil Sci.* **2016**, *179*, 574−583.
(32) Schiedung, H.; Tilly, N.; Hütt, C.; Welp, G.; Brüggemann, N.; Amelung, W. *Geoderma* **2017**, *303*, 44−51.
(33) Jeong, S. H.; Borisov, O. V.; Yoo, J. H.; Mao, X. L.; Russo, R. E. *Anal. Chem.* **1999**, *71*, 5123−5130.
(34) Ohlsson, K. E. A. *Anal. Chem.* **2013**, *85*, 5326−5329.
(35) Werner, R. A.; Brand, W. A. *Rapid Commun. Mass Spectrom.* **2001**, *15*, 501−519.
(36) Werner, R. A.; Bruch, B. A.; Brand, W. A. *Rapid Commun. Mass Spectrom.* **1999**, *13*, 1237−1241.
(37) Borisov, O. V.; Mao, X.; Russo, R. E. *Spectrochim. Acta, Part B* **2000**, *55*, 1693−1704.
(38) Bleiner, D.; Plotnikov, A.; Vogt, C.; Wetzig, K.; Günther, D. *Fresenius' J. Anal. Chem.* **2000**, *368*, 221−226.
(39) Paul, E. A.; Follett, R. F.; Leavitt, S. W.; Halvorson, A.; Peterson, G. A.; Lyon, D. J. *Soil Sci. Soc. Am. J.* **1997**, *61*, 1058−1067.
(40) Holz, M.; Zarebanadkouki, M.; Kuzyakov, Y.; Pausch, J.; Carminati, A. *Ann. Bot.* **2018**, *121*, 61−69.

DOI: 10.1021/acs.analchem.9b00892
Anal. Chem. 2019, 91, 6225−6232